An outer membrane-inspired polymer coating protects and endows *E. coli* with novel functionalities

Andrea Belluati*[a], Iain Harley[b], Ingo Lieberwirth[b], Nico Bruns*[a]

[a] Dr. A. Belluati, Prof. Dr. N. Bruns.
Department of Chemistry
Technical University of Darmstadt
Alarich-Weiß-Straße 4, 64287 Darmstadt
Germany
E-mail: andrea.belluati@tu-darmstadt.de; nico.bruns@tu-darmstad.de

[b] I. Harley, Dr. I. Lieberwirth
Department of Physical Chemistry of Polymers
Max Planck Institute for Polymer Research
Ackermannweg 10, 55128 Mainz
Germany

Supporting information at the end of the document.

Abstract: A bio-inspired membrane made of Pluronic® L-121 is produced around *E. coli* thanks to the simple co-extrusion of bacteria and polymer vesicles. The block copolymer-coated bacteria can withstand a variety of harsh shocks, e.g. temperature, pressure, osmolarity and chemical agents. The polymer membrane also makes the bacteria resistant against enzymatic digestion and enables them to degrade toxic compounds, improving their performance as whole-cell biocatalysts. Moreover, the polymer membrane acts as a new region for surface modification. Being decorated with α-amylase or lysozyme, the cells are endowed with the ability to digest starch, or self-predatory bacteria are created. Thus, without any genetic engineering, the phenotype of encapsulated bacteria is changed, as they become sturdier and gain novel metabolic functionalities.

Introduction

In nature, the great majority of uni- and multicellular organisms is composed of cells whose membranes are surrounded by additional protective layers, generically named cell wall, found in most prokaryotes, fungi, algae, and plants. The cell wall provides structural support and resistance from external stressors, regardless of its diverse chemical structures.[1] Synthetic coatings composed of multiple protective layers have been extensively developed, for instance as delivery devices for encapsulated small

molecules and particles.[2] A natural progression was to encapsulate -or coat- living cells within natural and/or synthetic materials, affording protection, and separation from the outside environment.[3] Cell encapsulation refers to a broad range of immobilization techniques that entrap cells within well-defined matrixes, often overlapping with cell coating.[4] It provides cytoprotection,[3a] and can be used for cell delivery,[5] but also to co-culture different strains and species for industrial applications.[6] These techniques, for the greatest part, rely on the encapsulation of several cells per object, be it capsule, hydrogel, droplet and so forth, entrapping the equivalent of small cellular populations, or biofilms in the case of bacteria. Albeit with obvious advantages, such as a higher payload per unit and ease of recovery, the main shortcoming of multi-cell encapsulation is that of any multicellular organism, where a lower surface/volume ratio decreases the mass transfer rate for metabolites.[7] To this end, single-cell encapsulation, originally developed as a way to segregate and analyse heterogeneous cell populations,[8] and to improve cell delivery systems,[9] offers an opportunity to link the optimal compound exchange offered by the high surface-to-volume ratio, with the physical enhancement that cell encapsulation can provide. In this regard, both animal cells and eukaryotic microbes (*e.g.*, yeasts, diatoms) have been encapsulated within droplets or vesicles,[8] polymeric microgels,[9] or within capsules made of polyphenols,[4] and inorganic compounds.[10] Single prokaryotes have also been encapsulated in a variety of materials: mainly polymers,[11] organic-inorganic composites,[11f, 12] and graphene,[13] to improve their utility both as delivery vectors and whole-cell catalysts. A peculiar strategy is to co-extrude erythrocytes together with *E. coli*, exploiting the self-assembly of the phospholipid membrane of the erythrocytes to reform an additional membrane around the bacteria, allowing them to act as stealthy, living therapeutics.[14] However, this approach relies on unstable, immunogenic phospholipid membranes of biological origin, limiting the spectrum of applications. We thus turned our attention to amphiphilic block copolymers as synthetic mimics of phospholipids, which offer additional physical resistance, chemical versatility and biocompatibility.[15] We selected the well-known, inexpensive, amphiphilic triblock copolymer Pluronic® L-121 (PL121, poly(ethylene

glycol)-*block*-poly(propylene glycol)-*block*-poly(ethylene glycol), PEG_5-*b*-PPG_{62}-*b*-PEG_5)[12a] to form cell-sized giant unilamellar vesicles (GUVs)[16] that were extruded together with *E. coli* through a track-etched membrane creating an additional thin block copolymer membrane around the bacteria. This membrane not only increased the cell viability in a broad variety of physicochemical stresses, but also became a new anchor layer to decorate the bacteria with clickable moieties, effectively modifying their surface without any additional covalent bonds to the molecules on the cell. The surface-modified bacteria could be functionalized with bio-orthogonal exoenzymes (alpha-amylase, lysozyme) that altered their phenotype without any genetic manipulation. Our design creates robust and versatile bacteria to be applied in both white and red biotechnology.

Results and Discussion

Single-cell encapsulation

To develop an easy and adaptable encapsulation method, PL121 was chosen as membrane-building polymer. The amphiphilic triblock copolymer forms GUVs via a simple water/oil/water emulsion pipetting protocol.[17] After the solvent evaporation, the GUVs can be decorated with cholesterol-PEG_4-Cy5, which inserts efficiently into their membrane and allows their imaging (Figure 1a).[18] Different outer aqueous phases (sucrose solutions, phosphate buffered saline (PBS), cell culture medium) were tested, and all of them yielded GUVs. Their average size decreased as the salt content increased, with the growth medium Luria-Bertani (LB) yielding GUVs of a mean diameter <10 μm (Figure 1b). Mixing the formed vesicles with fluorescein confirmed that the membrane is intrinsically permeable to hydrophilic molecules in the range of a few hundreds of Da (Figure 1c).[19] We thus proceeded to mechanically extrude the bacteria and GUVs together in an Avanti mini-extruder,[14] where they passed through 1 μm-wide pores of a track-etched membrane, making the GUVs to burst and reassemble around the bacteria. The block copolymer membrane did not only encapsulate the bacteria, but also permitted their targeted decoration with cholesterol-PEG_4-Cy5 (Figure 1d, SI Figure 1).

Fluorescence imaging of YFP-expressing *E. coli* showed the fluorescence of Cy5 around the bacteria (Figure 1e, SI Figure 2). To further characterize the construct, 3 different polymer concentrations (w/v%; *E. coli*@0.034%, *E. coli*@0.051% and *E. coli*@0.062%, respectively) were tested, corresponding to increasing amounts of GUVs coextruded with bacteria (Table S1). Cryo-TEM shows an increase of the membrane thickness of encapsulated bacteria, ranging from 4 to 9 nm as the polymer concentration increased (Figure 1f). These values are lower than what was previously reported for the thickness of the polymer membrane of PL121 GUVs (11 nm),[20] suggesting that the polymer on the bacterium is not stretched and "floating" around the cell, but rather interacts with the bacterial outer surface, forming a dense membrane made of heavily coiled polymer chains, as previously reported for block copolymers with a >2000 Da hydrophobic chain.[21] The ζ-potential of encapsulated bacteria was closer to that of GUVs than to that of naked bacteria, but still more electronegative (Figure 1f), whereas bacteria simply mixed with GUVs maintain a strongly electronegative ζ-potential (SI Figure 4). After 4 h at 37 °C, the ζ-potential of the polymer-encapsulated cells decreased as well, possibly because of the growth of bacteria that eventually break free of their synthetic membrane. A complete coverage of the polymer by the membrane would completely mask the surface charge of the cells; however, the lack of any visible domain or blotchy coating in both CLSM and cryo-TEM (SI Figure 3) suggests a total coating of the surface by the polymer (Figure 1g), which however remains permeable and does not completely mask the bacterium's surface charge. The enwrapping was further confirmed by a slightly hindered proliferation on agar (SI Figure 5a). No damage to the bacterial membrane was detected, as plasmids were not lost over time in a plasmid retention assay (SI Figure 5b). Overall, these results show that the bacteria were enwrapped by a thin polymeric membrane that influenced their surface features and their proliferation. Interestingly, the amount of polymer needed for encapsulation was orders of magnitude lower than what was used for encapsulation of bacteria in Pluronic-based hydrogels,[22] suggesting a higher biological and environmental compatibility of the constructs.

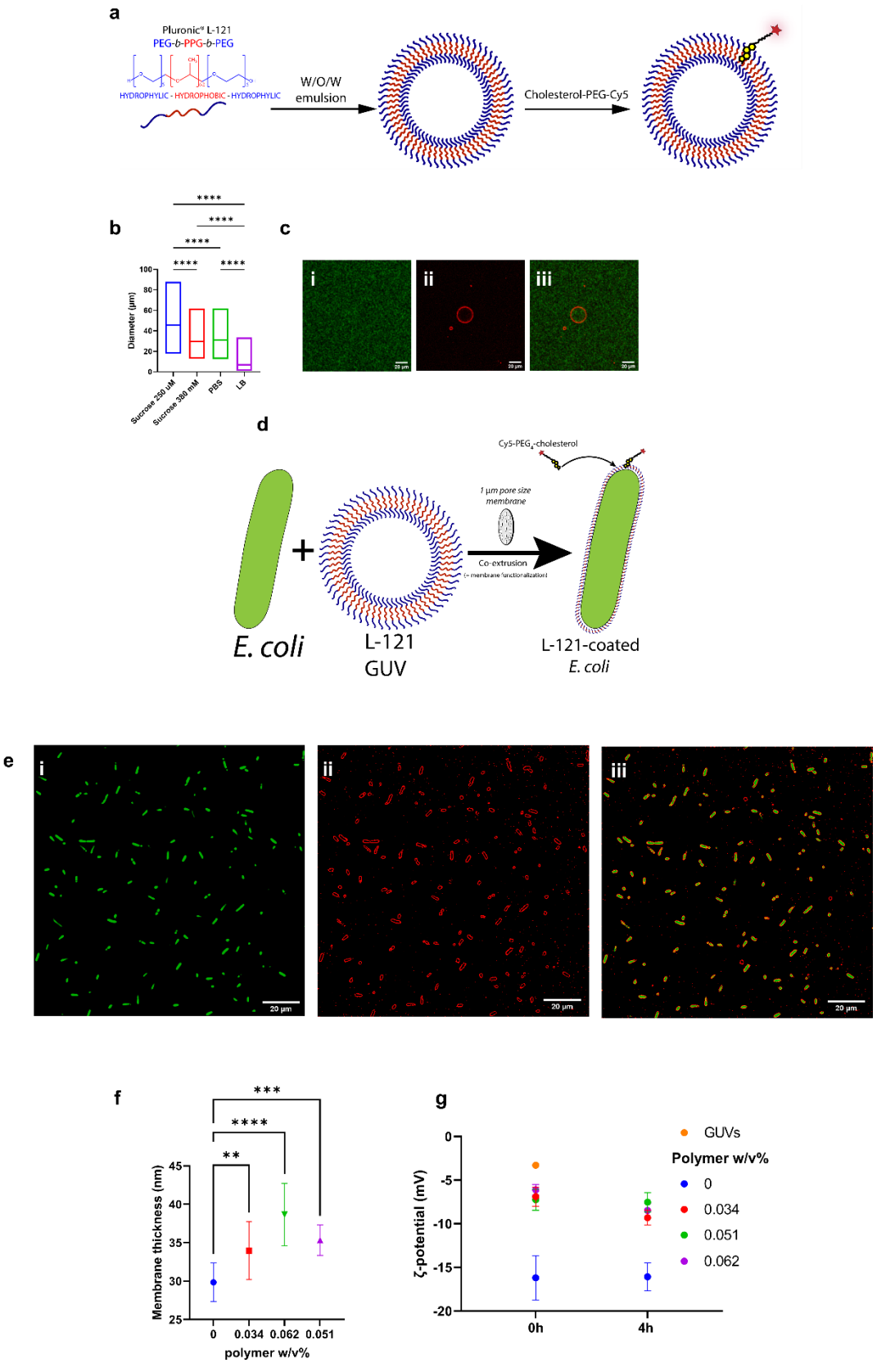

Figure 1. a) Schematic of the production of PL121 GUVs and their fluorescent tagging with cholesterol-PEG_4-Cy5. b) Mean distribution of the resulting GUVs in different outer

water phases (±S.D., n≥50 GUVs). c) Representative confocal laser scanning microscopy (CLSM) micrograph of GUVs (i: fluorescein; ii: Cy5-labeled membrane; iii: overlay). d) Schematic of *E. coli* coating with PL121 via bacteria co-extrusion with GUVs. e) CLSM micrograph of PL121 coated bacteria (i: YFP-expressing *E. coli*; ii: Cy5-labeled polymer membrane; iii: overlay). f) Membrane thickness (cell wall + polymer) (mean, ±S.D., n=20 sections) measured from cryoTEM micrographs. g) ζ-potential (mean, ±S.D., n=3) of naked and PL121 encapsulated bacteria at different w/v% and pure GUVs, right after sample preparation and 4 h later. **: $p<0.01$; ***: $p<0.001$ ****: $p<0.0001$.

Cell metabolism and protection upon encapsulation

Having established a protocol for the encapsulation of the bacteria in a thin polymer membrane, the influence of the encapsulation on the cell metabolism was investigated next. Three optically measurable biomarkers were selected: the well-known viability assay via the conversion of fluorescein diacetate (FDA) to fluorescein; the optical density at 600 nm (OD_{600}) as a measure of the bacterial growth; and the fluorescence of NAD(P)H as an indication of the overall redox potential of cells (Figure 2a). The FDA metabolism decreased with increasing polymer concentration, most likely because the shell increased in thickness, slowing down the diffusion of the substrate to the bacteria. The OD_{600} decreased with increasing polymer concentration, i.e. cell division decreased, most likely because the weak mechanical constraint of the polymer membrane hindered cell division (Figure 2b). NAD(P)H levels, however, increased with higher polymer concentrations, as the decreased cell proliferation meant that more reducing energy was available within the cells (Figure 2c), which is in line with results from previous cell encapsulation studies.[7b]

The encapsulation of microorganisms has been shown to protect cells from several physicochemical stressors,[4] a very beneficial feature for any industrial application. To investigate the protection effect of the PL121 membrane on the cells, encapsulated bacteria were subjected to several harsh conditions and their FDA conversion was

compared, as a viability stand-in, to naked bacteria in the same conditions. The encapsulation in a P121 membrane increased the cell viability when stressed with high and low temperatures. This was particularly pronounced (up to 50% viability increase) at lower polymer concentrations, possibly due to temperature-dependant modifications of Pluronic packing and permeability, inducing the collapse and compaction of chains.[23] The shell also protected against mechanical stresses, such as high-speed centrifugation and ultrasonication. When subjected to osmotic stress, polymer-enwrapped cells were more protected than their naked counterparts if put in a hypoosmotic environment (MilliQ water), whereas no detectable improvement occurred for a hyperosmotic medium (1 M sucrose), evidencing that the polymer membrane could withstand cell swelling, but was unable to help against cell shrinkage. Against chemical agents (70% EtOH and 20% H_2O_2, respectively), a thicker shell provided better protection, most likely because it limited diffusion of the chemical agents to the cell. (Figure 2d, SI Table 2).

For comparison, bacteria were mixed with GUVs but not co-extruded, and subjected to harsh temperatures and centrifugation. The simple presence of the GUVs did not increase viability (Figure 2d), indicating that the polymer has to form a membrane around the polymers in order to efficiently protect it.

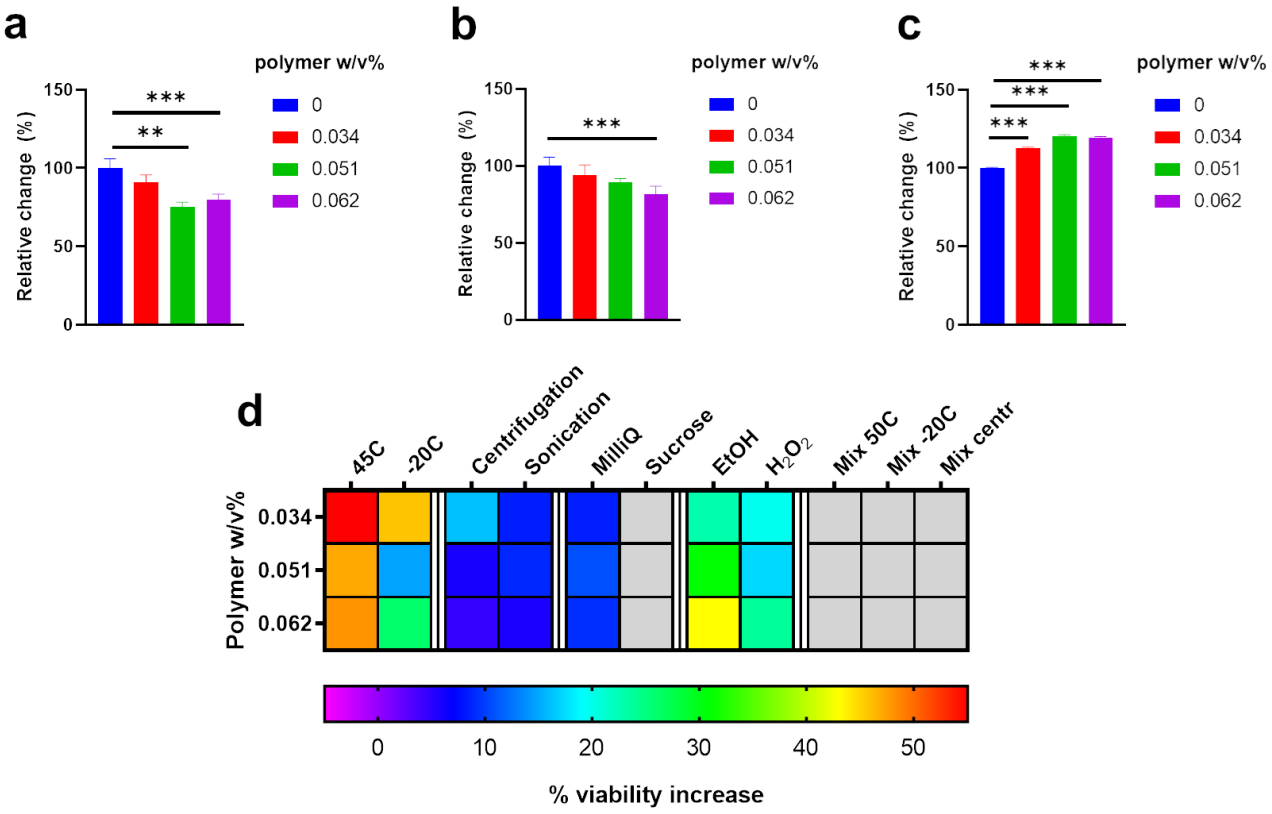

Figure 2. a) Relative change in FDA conversion of naked and PL121-encapsulated bacteria (mean, ±S.D., n=3). b) Relative change in OD_{600} of naked and encapsulated bacteria (mean, ±S.D., n=3). d) Relative change in NAD(P)H content of naked and encapsulated bacteria (mean, ±S.D., n=3). d) Heatmap of the % viability change (expressed as FDA conversion) of encapsulated bacteria compared to naked bacteria, when subjected to a selection of harsh conditions. Values below -5% were assigned grey colour. The numerical values are reported in table SI Table 2. **: $p<0.01$; ***: $p<0.001$.

Having demonstrated the protective effect of the polymer coating, we moved on to a more complex model application, where an engineered whole cell biocatalyst (WCB) would be stressed with several temperature shocks, *i.e.* simulating mishandled storage conditions or multi-step reaction cycles. The possibility to induce protein production in the polymer-coated bacteria was confirmed (SI Figure 6). Then, myoglobin (Mb)-producing bacteria were coated with the polymer and subjected to a heat-cold-heat cycle.

The coated WCBs were washed, resuspended in new medium, and Mb expression was induced. The peroxidase activity of Mb was confirmed by the production of coloured ABTS radicals (SI Figure 7) and by luminescence occurring from the oxidation of luminol (Figure 3a, SI Figure 8).[24] While untreated, naked bacteria do have a catalytic advantage against encapsulated *E. coli*@0.062 % bacteria, they lose their activity once subjected to the harsh heat-cold-heat treatment, whereas the encapsulated Mb-expressing bacteria only suffer a minor decrease in catalytic activity (Figure 3b). Finally, we applied the coating's protection against chemical agents to a model WCB detoxification process, using the dehalogenation activity of peroxidases. Mb-producing bacteria were used to convert the mutagenic and carcinogenic 2,4,6-trichlorophenol (2,4,6-TCP) to its less toxic hydroxyquinone derivative.[25] using H_2O_2 which was either added directly, or produced *in situ* by glucose oxidase. By monitoring the absorbance of 2,4,6-TCP, of the intermediate 2,6-dichloroquinone (2,6-DCQOH), and of the end product 2,6-dichlorohydroxyquinone (2,6-DCQOH), we could progressively observe the conversion of 2,4,6-TCP to a more hydrophilic compound, The experiments demonstrated a synergy between encapsulation and a slow H_2O_2 feed that allowed the bacteria to detoxify their medium and increase their biomass (SI Figure 9).

The polymer membrane on the bacteria also protects the cells from macromolecular degrading agents, namely the bacteriolytic lysozyme. Gram-negative *E. coli* is susceptible to this hydrolase enzyme. The membrane made the bacteria more resistant (Figure 3c). As the polymer concentration increased, the advantage over naked bacteria with higher concentrations of lysozyme increased, reaching an 8-fold improvement in bacterial vitality for the highest concentration of enzyme with the highest concentration of polymer (Figure 3d). This resistance to lysozyme was applied to a model of a culture contamination, where lysozyme might be used to selectively eliminate unencapsulated bacteria (the contaminant), while encapsulated ones should be retained. To test this hypothesis, non-fluorescent, unencapsulated bacteria were mixed with the same strain that was enwrapped in polymer and expressed fluorescent YFP. As unencapsulated bacteria can grow unhindered by the encapsulation, they will tend to outgrow their

fluorescent counterparts, thus the ratio between fluorescent signal (only one population) and OD_{600} (both populations) will decrease over time. A selective antimicrobial, such as lysozyme, will be able to counter this phenomenon (Figure 3e). When unencapsulated bacteria were mixed in a 10:1 ratio to encapsulated ones, we could observe how, in the absence of lysozyme, the YFP/ OD_{600} ratio would quickly drop over time. However, it remained constant in presence of lysozyme (Figure 3f). Moreover, the resulting cell debris was a confirmation of lysozyme's action (SI Figure 10). If we instead prepared a 100:1 population ratio, the lysozyme could not stop the outgrowth of unencapsulated bacteria but slowed it down markedly (Figure 3g). Thus, the polymer membrane selectively protected the encapsulated bacteria and can be used, in combination with externally added lysozyme, to remove unwanted microbes.

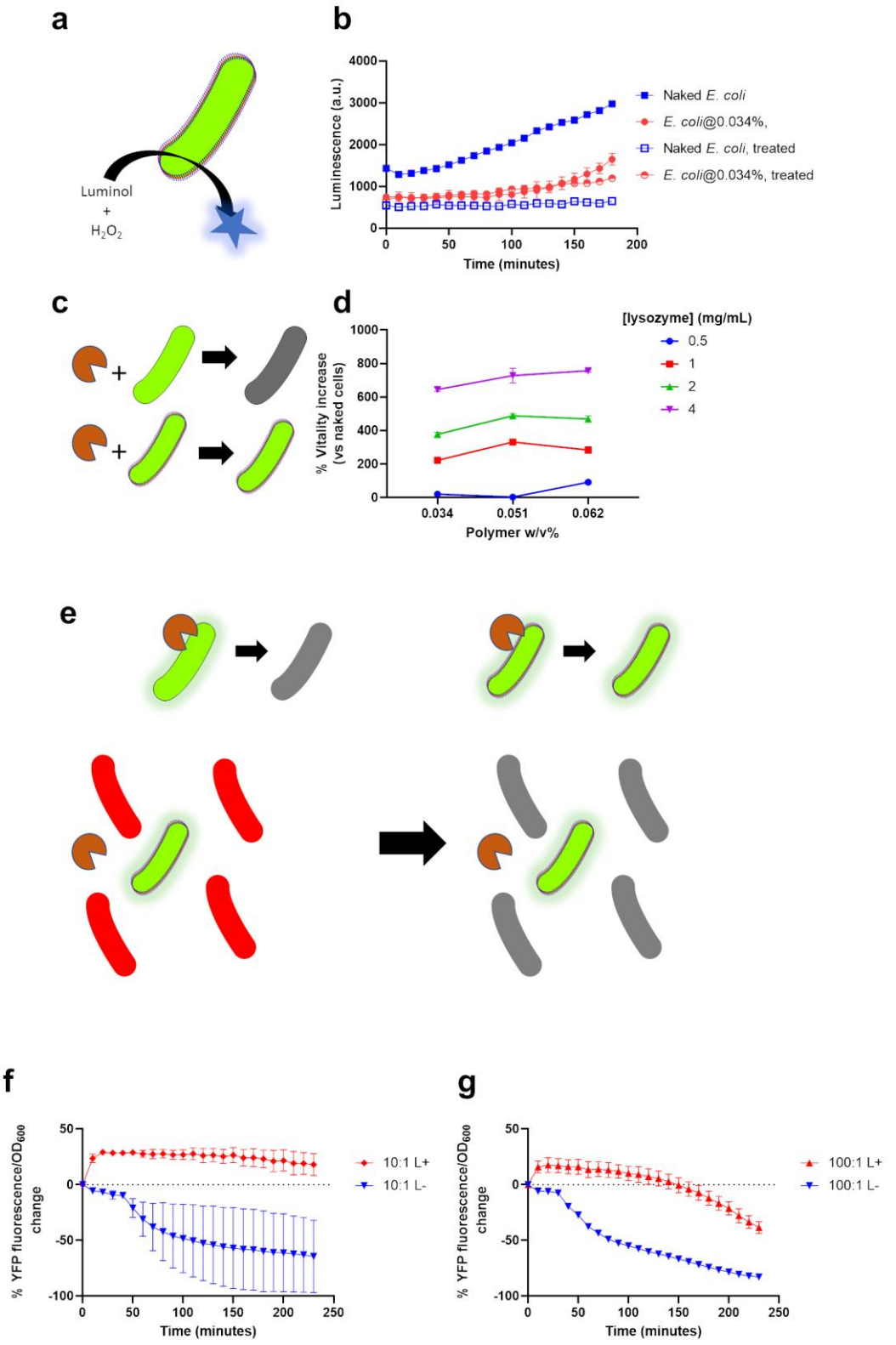

Figure 3. a) Schematic of the production of luminescence via Mb-expressing bacteria. b) Luminescence profile of naked and encapsulated Mb-producing bacteria (*E.*

coli@0.034%), as base activity and after treatment with a series of temperature and mechanical shocks (mean, ±S.D., n=3). c) Schematic of the effect of lysozyme on naked and PL121 encapsulated bacteria. d) Vitality increase of encapsulated bacteria when exposed to increasing concentrations of lysozyme (mean, ±S.D., n=3). e) Schematic of the action of lysozyme on naked, non-fluorescent bacteria and encapsulated, fluorescent bacteria (*E. coli*@0.062%) and of the YFP/OD_{600} assay to evaluate the discriminating activity of lysozyme in mixed populations. f) YFP/OD_{600} profile in a mixed population (10:1 naked:encapsulated) with (L+) and without (L-) lysozyme (mean, ±S.D., n=3). g) YFP/OD_{600} profile in a mixed population (100:1 naked:encapsulated) with (L+) and without (L-) lysozyme (mean, ±S.D., n=3).

Membrane decoration with exoenzymes

The polymer membrane does not only protect the cells, but it also offers a convenient anchor for surface decoration with various molecules. One example was the insertion of Cy5 to label the membrane, via its conjugation to a cholesterol-PEG_4 anchor. Moreover, cholesterol that bears clickable moieties allows to easily modify the bacteria's new membrane, and thus the surface of the polymer-encapsulated bacteria, with a wide array of interesting biomolecules.[18, 26] One possibility is the functionalization of the cell surface with non-native exoenzymes, effectively modifying their surface reactivity without the need for genetic engineering.[27] For instance, *E. coli* does not excrete α-amylase (αAM),[28] an enzyme that digests starch to maltose. By conjugating αAM to cholesterol-PEG_4, followed by cholesterol insertion into the encapsulating membrane , the surface of the polymer-encapsulated bacteria was decorated with the enzyme, allowing *E. coli* to proliferate on starch alone (**Figure 4**a). Encapsulated bacteria without amylase grew less than naked ones without amylase, and slightly better in the presence of free amylase. However, if the encapsulated bacteria were decorated with αAM-cholesterol, their growth improved compared to naked ones. Thus, the enzyme on the surface readily delivered maltose to the cells. The cells were furthermore centrifuged and

washed to remove any αAM that was not attached to the polymer membrane. Without cholesterol, encapsulated cells performed again worse than the naked ones, whereas polymer-enwrapped bacteria that were modified with cholesterol-PEG_4-αAM retained most of their viability (**Figure 4**b). These results confirmed that the synergy between an additional membrane and an exoenzyme functionalized with cholesterol endowed the bacteria with a novel metabolic capability.

Carbohydrate digestion was not the only possibility, however. In nature, some bacteria such as *Bdellovibrio bacteriovorus* prey on other bacterial species, including pathogenic ones, and are thus being researched as interesting antibiotic alternatives.[29] Inspired by this kind of bacteria, we modified cholesterol-PEG_4 with lysozyme and decorated the surface of polymer-enwrapped *E. coli* with it (**Figure 4**c). In this way, the bacteria themselves become armed with a molecule that kills their unarmoured equivalents. Surface-functionalized fluorescent bacteria were mixed with naked, non-fluorescent ones. The ratio between fluorescence and OD_{600} is an indicator of the encapsulated bacteria fraction in the culture. The ratio dropped quickly in absence of lysozyme (i.e. the naked bacteria grow faster), but was slower to decrease when the encapsulated bacteria were equipped with the enzyme on their surface and could counteract the others' growth (**Figure 4**d). However, the ratio eventually decreased in this case too, indicating that the surface-bound lysozyme could not easily reach other bacteria, relying instead on two bacteria being close enough in order for the lysozyme to act and kill the other bacteria.

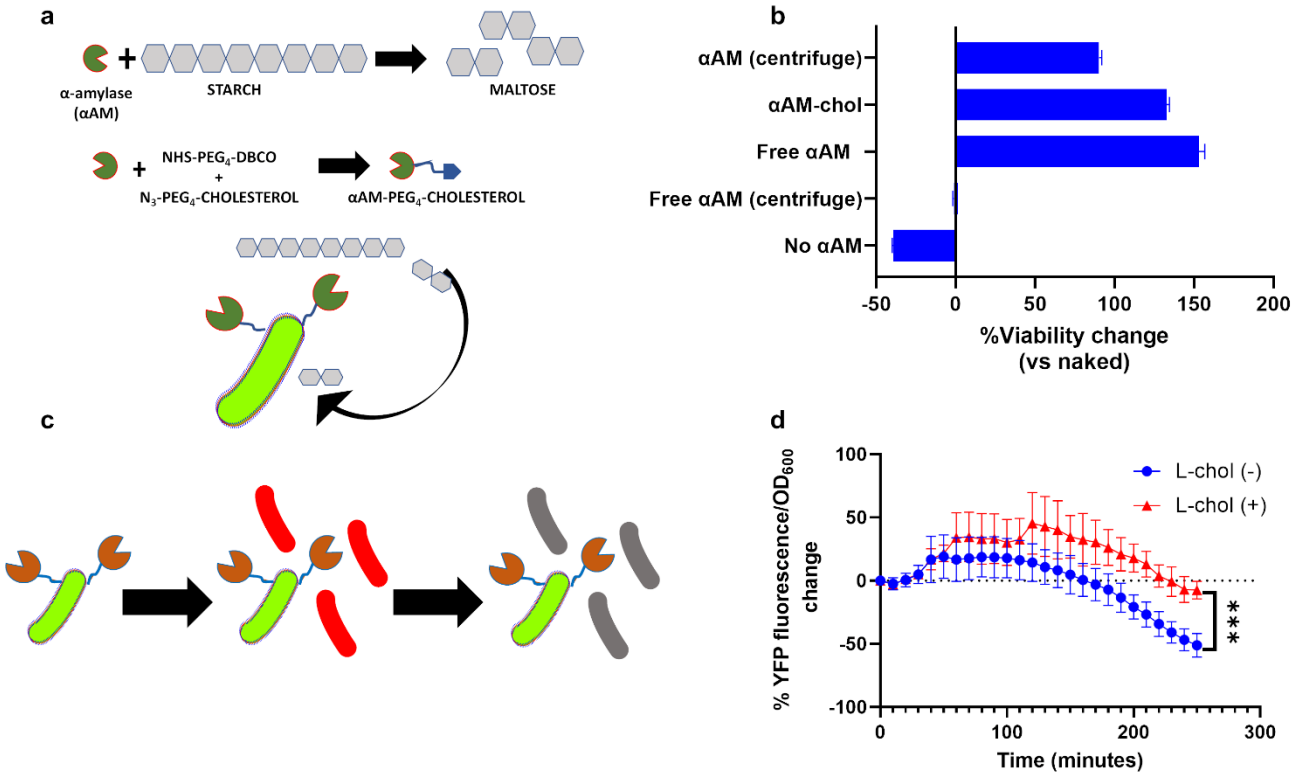

Figure 4. a) Schematic of the mechanism of αAM and its functionalization onto the surface of bacteria, allowing digestion of starch by *E. coli*. b) Viability change of encapsulated and naked bacteria growing on starch alone, with free αAM or αAM on their surface (αAM-chol) (mean, ±S.D., n=3). c) Schematic of the functionalization of lysozyme onto the surface of bacteria and its action against naked bacteria. d) Variation of YFP/OD_{600} profile overtime for a mixed population of encapsulated, fluorescent and lysozyme-equipped bacteria (L-chol (+)) and naked bacteria, showing the slowing down of outgrowth of the latter by the former (mean, ±S.D., n=3). ***: $p<0.001$

Conclusion

We have developed a simple singe-cell encapsulation process using amphiphilic block copolymers that form a thin cell-wall like structure around individual cells. This allowed *E. coli* to resist a wide array of degrading agents, and protected it against hydrolytic enzymes that, therefore, selectively inactivated non-encapsulated bacteria. Moreover, the block copolymer membrane acted as an anchor for surface modifications of the bacteria with exoenzymes, allowing the bacteria to grow on non-canonical macromolecular nutrients, or to become predators with the ability to kill their unencapsulated counterparts. Thus, encapsulation of bacterial cells with an amphiphilic block copolymer membrane and surface functionalization of this synthetic layer allows to change the phenotype of cells, making them able to withstand various cell-toxic agents and physical stresses, without any genotype modification. Such a bio-inspired coating could find applications in industrial and environmental biotechnology, e.g. to allow the use of WCBs in previously unfavourable environments. Moreover, polymer-enwrapped cells could also be useful in biomedical research, synthetic biology and for engineered living materials, as the easy functionalization of their surface consents the decoration with a plethora of molecules, with applications ranging from targeting to surface adhesion, exocellular catalysis and selective killing.

Acknowledgements

This project has received funding from the European Union's Horizon 2020 research and innovation programme under the Marie Skłodowska-Curie grant agreement No. 101032493. I.H. acknowledges support from the EU SuperCol Project under grant agreement No. 675179. The authors wish to acknowledge Dr. Brigitte Hertel for her help in electron microscopy characterization, Prof. Wolf-Dieter Fessner for the provided strain, Dr. Aaron K. Lau for providing

access to his facility, and Michael Kickstein and Eleonora Ornati for assistance with bacterial cultures.

Keywords: single-cell encapsulation • block copolymers • membranes • cytoprotection • membrane functionalization

Experimental Section

Materials and strains

Unless otherwise specified, all reagents were purchased from Merck and used as received. Poly(ethylene glycol)-*block*-poly(propylene glycol)-*block*-poly(ethylene glycol) (Pluronic® L-121; average M_n ~4400, composition: 30% PEG) is a product of BASF SE and was purchased from Merck. The used strain was *E. coli* BL21 (DE3), which was purchased from Thermo Fisher and was used to transform all the plasmids. YFP was encoded in the plasmid pETTherm α/β,[30] sperm whale myoglobin (swMb, wild type) was in the plasmid pet-20b(+). The empty pet-26b(+) vector was a donation from Prof. Wolf-Dieter Fessner (Technical University of Darmstadt).

Preparation of GUVs

The GUVs were prepared according to a scaled-up published protocol.[17] Pluronic® L-121 was dissolved in toluene at 20 mg ml^{-1}. 20 µl of 380 mM sucrose were added to 150 µl of toluene, and mixed by vigorous pipetting for 1 minute (w/o emulsion). 175 µl of the w/o emulsion were then pipetted into 1.2 ml of outer water phase (either 380 mM sucrose solution, PBS or LB medium) and pipetted again for 1 minute. The solvent was left to evaporate under very mild air flow for 2 h.

Bacterial growth and protein expression

All strains were grown in 5-10 ml of LB medium (10 g tryptone, 5 g yeast extract, 10 g NaCl, 1 l ddH_2O) at 37 °C, supplemented with the antibiotic their plasmids encode the resistance for. Protein expression (YFP and myoglobin) was induced at OD_{600} 0.6 with 0.1 mM isopropyl β-D-1-thiogalactopyranoside (IPTG) and 0.1 mM 5-aminolevulinic acid.

Bacterial encapsulation

Bacteria were grown to OD_{600} 1. They were then diluted to OD_{600} 0.5 in fresh LB right before extrusion. Volumes of GUVs and bacterial suspensions were adjusted to obtain 1.1 ml of mixture at three different PL121:bacteria volume ratios (1:1, 3:1, 9:1), corresponding to the weight/volume% of 0.034%, 0.051%, 0.062% (SI Table 1). Then, 1 ml of these adjusted mixtures was pipetted into the syringe of a Mini Extruder (Avanti, USA) equipped with Whatman® Nuclepore® 1 μm track-etched membrane filters (VWR, Germany), and passed through for 12 times.[14] In this way, GUVs would break up passing through the pores, reforming around the bacteria extruded together with them.

The same ratios were used for mixed bacteria and GUVs, skipping the co-extrusion step. Naked bacteria were also diluted in LB to a final OD_{600} 0.05. We assumed the equivalence OD_{600} 1 = 8×10^8 cells.

Plasmid retention assay

Naked and encapsulated bacteria with pet-26b(+) were plated on LB-agar. The agar plates were incubated at 37 °C for 16 h. Then, colonies were counted. 100 colonies of each were picked and stabbed on new plates with kanamycin, incubated at 37 °C overnight, and the number of grown colonies was counted again. Bacteria grown without selective pressure (antibiotic) and with a damaged membrane lose more easily their plasmid. Transferring them to a medium with the antibiotic will indicate what percentage lost their plasmid in the first step (*i.e.*, whether their membrane was damaged by the encapsulation).

Membrane labelling and CLSM imaging

1.6 μmol of cholesterol-PEG_4-N_3 were mixed with 4.8 μmol dibenzocyclooctyne-Cy5 (DBCO-Cy5) to 1 mL PBS and left to react at RT for 4 hours, then dialysed overnight (1 kDa MWCO) against PBS to remove unreacted dye. The intensity of the blue decrease only slightly after dialysis (visually confirmed), suggesting a good conjugation efficiency, and good retention by the dialysis membrane.

Samples were placed in Nunc® Lab-Tek® 8-well chamber slides (Thermo Fisher), 5 to 20 μl of sample in 200 μl PBS, with the addition of either 10 μl cholesterol- PEG_4-Cy5 or 10 μl 100 μM Nile Red (NR) in DMSO. To verify the membrane permeability, 10 μl of 1 mM sodium fluorescein in DMSO were added to the outside of the vesicles.

The imaging was done on a Leica SP8 CLSM, equipped with an HCX PL APO 63 × NA 1.2 W CORR CS2 objective (Fluorescein, YFP: ex. 488 nm, em. 505–525 nm; Nile Red: ex. 561 nm, em. 570–590 nm; Cy5: ex.635 nm, em. 660–690 nm).
For the sizing of GUVs, between 30 to 60 GUVs per sample were imaged.
Images were optimized (brightness and contrast; applied evenly throughout a whole image) and analysed via ImageJ.
Multiple comparison one-way ANOVA with Tukey correction was used to compare the populations.

CryoTEM

3 µl of the sample were placed onto a 400 mesh copper grid covered with lacey film (previously glow discharged). The grid was plunged into liquid ethane (automated plunging system, Vitrobot FEI) and transferred in liquid nitrogen to the TEM (Titan Krios G4, Thermo-Fisher Scientific) and micrographs were acquired using a Ceta 4k camera (Thermo-Fisher Scientific). The TEM was operated at 300 kV. Membrane thickness was then measured via ImageJ, n=10 different measurements.

ζ-potential measurement

50 µl of the sample were diluted into 1 ml PBS. Then, the ζ-potential was measured in a capillary flow cuvette with a Zetasizer Nano (Malvern). 3 repeated measurements were taken for all samples. Multiple comparison two-way ANOVA with Tukey correction was used to compare the populations.

Microplate measurements of bacterial cultures

Several biomarkers were measured on a Spark microplate reader (Tecan), in a Greiner transparent 96-well plate. Naked and encapsulated bacteria (10 µl) were diluted to final 200 µl in LB. Time run were measured at 37 °C, 4 hours, endpoint measurements were measure at RT.
The absorbance of fluorescein (from 0.05 mM FDA) was measured at 490 nm, OD_{600} at 600 nm, and NADPH fluorescence at 340/460 (±20) nm. Kinetic curves were integrated, and their values averaged and compared (two-way ANOVA with Tukey correction). The viability increase (expressed by FDA hydrolysis) was used as a general indicator for encapsulation performance.

Cy5 and YFP fluorescence were measured at 620/682 nm and 485/535 nm (±20 nm), respectively. Multiple comparison two-way ANOVA with Tukey correction was used to compare the measurements.

Bacterial stressors

Depending on the experiment, bacteria were incubated 15 minutes at 45 °C, 1 h at -20 °C, centrifuged (12000 RCF in an Eppendorf microgentrifuge) for 30 min, sonicated with a Fisherbrand ultrasound probe (70 s, 5+5 second pulse, amplitude 50%), incubated 2 h in MillIQ water or 1 M sucrose, 30 min in 70% EtOH and 10 min in 20% H_2O_2, or a combination thereof. After incubation with chemicals, bacteria were gently centrifuged and resuspended in LB before measurements. Multiple comparison two-way ANOVA with Tukey correction was used to compare the measurements.

Activity of Mb-expressing *E. coli*

After 3 hours of swMb expression, bacteria were subjected to temperature + centrifugation shocks, and then mixed with 2 µl 0.01% H_2O_2 and 2 µL 0.1 mM ABTS; the production of the coloured ABTS radical cation was measured at 420 nm in the microplate reader. For the chemoluminescence, 100 µl 300 mM luminol substituted ABTS (whole luminescence spectrum recorded).

In the case of 2,4,6-TCP, 200 µl of bacteria were diluted to 1.5 ml LB with 50 mM 2,4,6-TCP and 1% H_2O_2 (H_2O_2 was otherwise substituted with 20 µl GOX 2 mg ml^{-1}) and incubated at 37 °C. Spectra from 240 to 700 nm were recorded (no replicates) at t= 0, 2 h and 4 h, in quartz cuvettes, in a Cary 60 UV-Vis spectrophotometer.

Lysozyme activity on bacteria

In plastic microcuvettes, naked and encapsulated bacteria (final OD_{600} 0.1, various polymer w/v%) were mixed with lysozyme at 0.5, 1, 2 and 4 mg ml^{-1} for 2 hours at 37 °C to a total volume 500 µl (with LB), supplemented with 2 mM EDTA. As lysozyme is a hydrolase, we did not use FDA but OD_{600} as biomarker of bacterial survival (Spark microplate reader). To this end, the final OD_{600} of naked bacteria subjected to the same lysozyme concentrations was set as 100%, and compared to the values of encapsulated bacteria.

The selective killing of naked bacteria was assayed as follows: YFP-expressing bacteria were encapsulated according to the protocol described above. They were mixed with naked, non-fluorescent bacteria at two ratios (10:1 and 100:1 in favour of naked bacteria), and incubated

with 4 mg ml^{-1} lysozyme for 4 hours at 37 °C in LB, supplemented with 2 mM EDTA. As OD_{600} reflects all bacteria, but YFP fluorescence comes only from the encapsulated population, the YFP/ OD_{600} ratio indicates the relative ratios in the mixture. Unencapsulated bacteria have a competitive advantage in growing, so without any selective killing, the ratio will decrease over time.

Surface functionalization with αAM

2 ml of a 2.5 mg ml^{-1} αAM solution in PBS was incubated with 45 µl of 10 mg ml^{-1} NHS-PEG_4-DBCO in PBS, for 4 hours at RT, then purified via a 40 kDa spin diafiltration device (Amicon, Merck) and further incubated overnight at 4 °C with 14.3 µl of 30 mg ml^{-1} cholesterol-PEG_4-N_3 in PBS, which was then spin filtered again. The concentration of αAM was measured by UV-vis spectroscopy at 280 nm using an extinction coefficient of 118 $mM^{-1}cm^{-1}$, calculated from the sequence as (N of tryptophan residues*5.5) + (N of tyrosine residues*1.5).[31] 100 µl of either PBS, αAM or αAM-PEG-cholesterol construct (at the same concentration) were mixed with 500 µl of bacteria. With or without a centrifugation step, 50 µl bacteria where then incubated for 4 h in 1 ml M9 minimal medium (Gibco) with 6.25 mg ml^{-1} of soluble starch, and OD_{600} was then measured. Multiple comparison two-way ANOVA with Tukey correction was used to compare the measurements.

Surface functionalization with lysozyme

The functionalization with lysozyme was conducted in the same manner as with AAM (using 5 mg ml^{-1} lysozyme). Fluorescent, encapsulated bacteria with lysozyme-cholesterol (*E.coli*@0.62%) were mixed 1:10 in their favour with naked, non-fluorescent bacteria, and the YFP/ OD_{600} ratio was measured during the course of 4 h. Multiple comparison two-way ANOVA with Tukey correction was used to compare the measurements.

Supporting Information

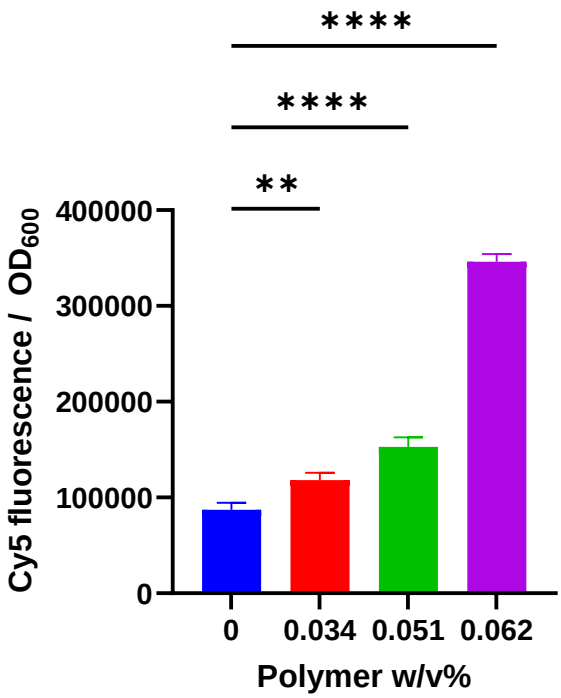

SI Figure 1. Fluorescence/OD_{600} after centrifugation. A higher value means that more of the membrane label Cy5-PEG_4-cholesterol is retained by each cell. Data displayed as mean ±S.D., n=3. **: p<0.01; **: p<0.001 ****: p<0.0001.

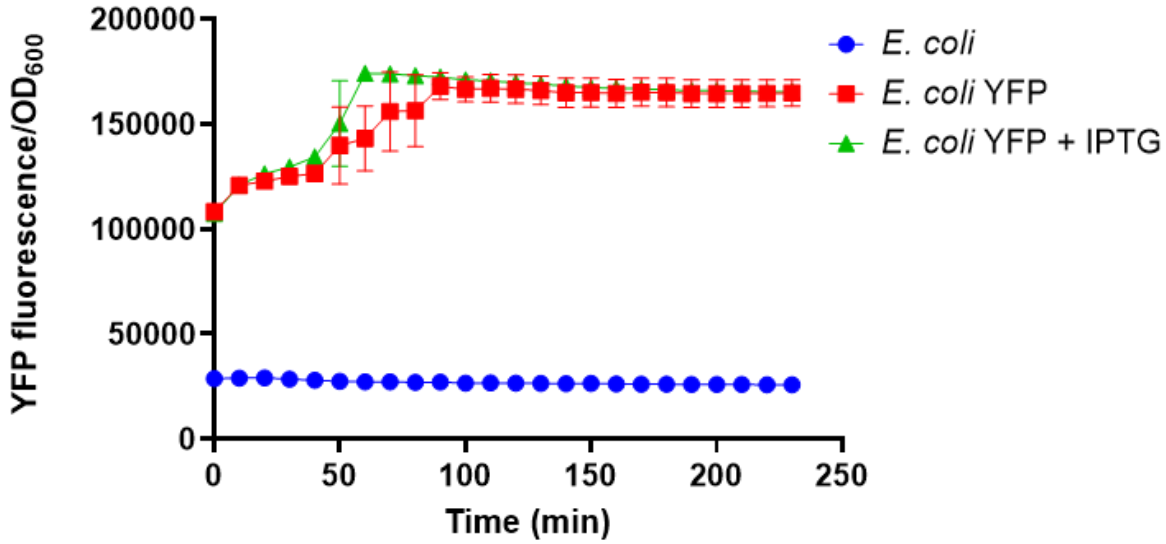

SI Figure 2. Fluorescence (normalized per cell) of plasmid-less *E. coli*, *E. coli* expressing YFP with and without induction, showing a detectablee fluorescence already before IPTG induction. Data displayed as mean ±S.D., n=3.

SI Table 1. Overview of the weight/volume% ratios used in this study, and their equivalents in volumes weight/weight of cell and femtomoles per cell.

Polymer weight/volume%	**PL121:bacteria (final OD 0.05) (volume ratio)**	**Polymer:cell (mg/mg)**	**Polymer:cell (fmol/cell)**
0.034%	1:1	9	2
0.051%	3:1	12	3
0.062%	9:1	15	4

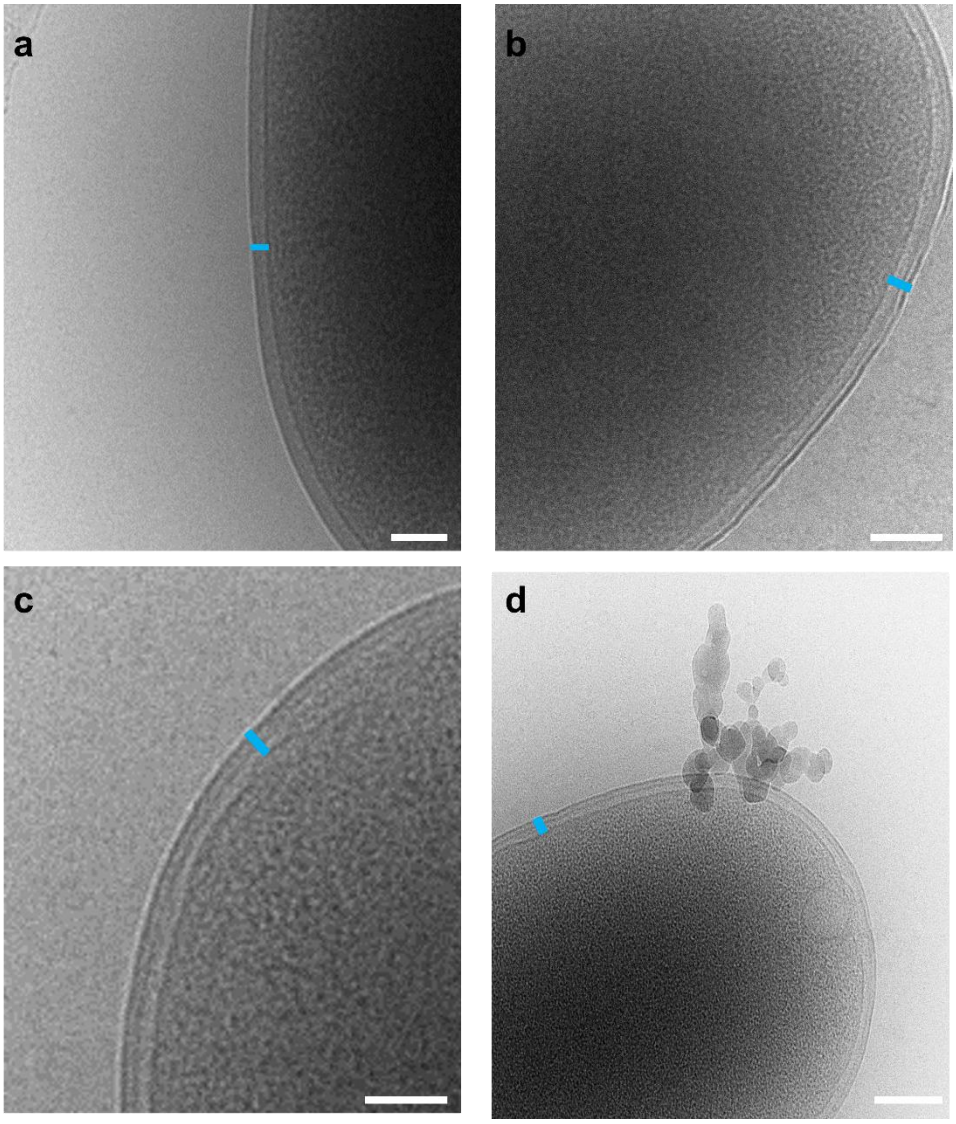

SI Figure 3. Cyro-TEM micrographs, showing membranes of *E. coli* and representative measured thicknesses**:** a) Membrane of a naked *E. coli*, the blue line is 33.2 nm. b) *E.coli*@0.034%, the blue line is 35.4 nm. c) *E.coli*@0.051%, the blue line is 39.1 nm. d) *E.coli*@0.062%, the blue line is 40.75 nm. A mass of additional polymer is visible on this bacterium. All scale bars are 100 nm.

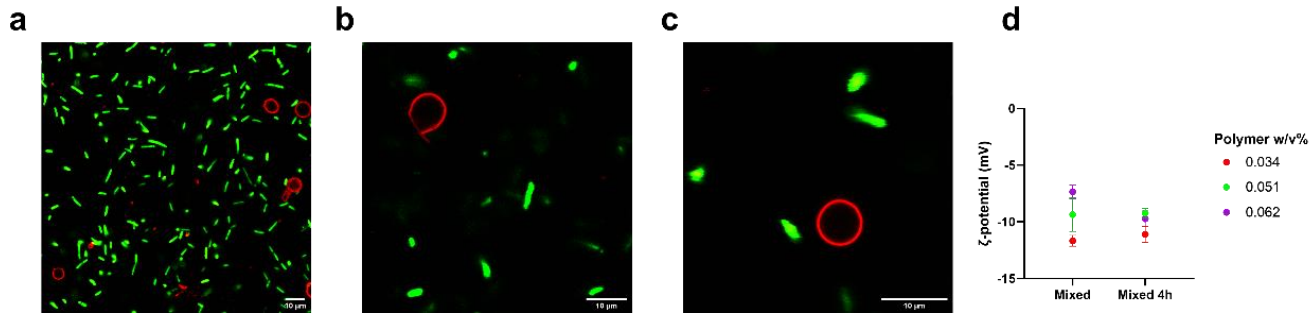

SI Figure 4. a-c) CLSM micrographs of YFP bacteria mixed with Cy5-presenting GUVs, showing the preferential insertion of the fluorophore in the polymersomes (overlays of YFP, green, and Cy5, red; scale bars = 10 µm). d) ζ-potential (mean, ±S.D., n= 3) of bacteria mixed with GUVs, without co-extrusion, right after sample preparation and 4 h later.

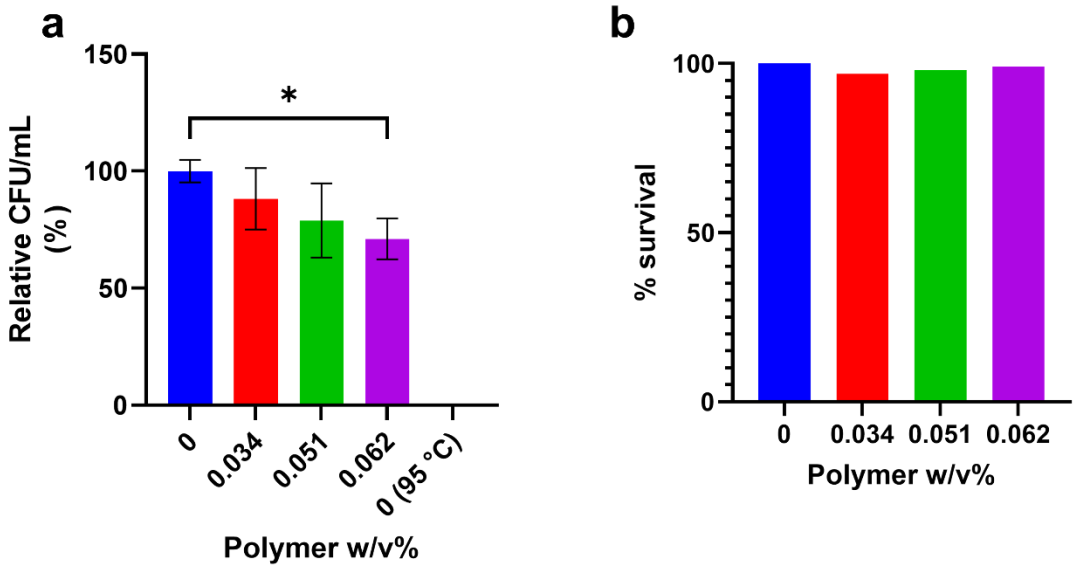

SI Figure 5. a) Relative CFU/mL of naked and encapsulated bacteria, showing a small effect of encapsulation on cell proliferation (naked bacteria in hot water as negative control). Data displayed as mean ±S.D., n= 3 (a), n= 100 colonies (b). *: $p<0.1$. b) Plasmid retention test, where bacteria with an intact membrane do not lose their plasmid and can thus survive on the corresponding selection antibiotic (single measurement).

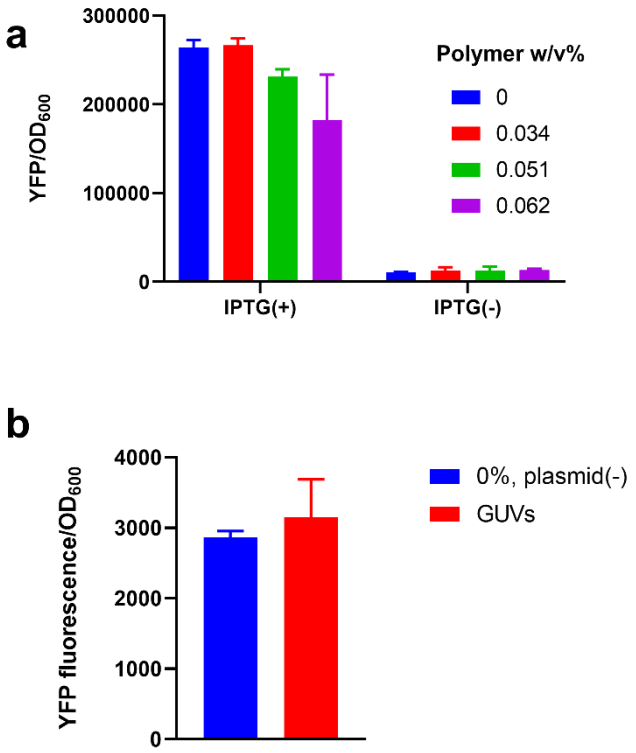

SI Figure 6. a) YFP fluorescence/OD_{600} cells (naked and encapsulated) with and without IPTG, showing that encapsulation still allows induction of protein expression. b) Negative control of the signal by plasmid-less bacteria and pure GUVs. Data displayed as mean ±S.D., n= 3.

SI Table 2. % viability increase (or decrease) of encapsulated cells compared to naked cells at different conditions (mean ± S.D., n=3).

	Polymer w/v%		
	0.034	0.051	0.062
45 °C	55.03 ± 7.76	47.11 ± 7.05	48.09 ± 6.49
-20 °C	45.79 ± 10.65	14.69 ± 8.22	25.99 ± 9.23
Centrifugation	16.09 ± 2.35	5.86 ± 5.30	4.54 ± 5.40
Sonication	8.33 ± 1.53	8.83 ± 6.00	5.69 ± 6.08
MilliQ	8.42 ± 0.46	10.73 ± 5.01	9.16 ± 5.11
Sucrose	-47.61 ± 1.39	-46.45 ± 5.27	-51.82 ± 4.12
EtOH	22.85 ± 1.82	30.94 ± 7.29	42.99 ± 8.00
H_2O_2	19.80 ± 1.79	17.18 ± 5.81	23.84 ± 5.47
Mix 50C	-20.30 ± 1.15	-30.94 ± 4.41	-28.38 ± 4.71
Mix -20C	-9.90 ± 1.94	-12.29 ± 4.98	-7.92 ± 5.40
Mix + centrifuged	-12.85 ± 3.56	-48.66 ± 4.38	-69.03 ± 3.80

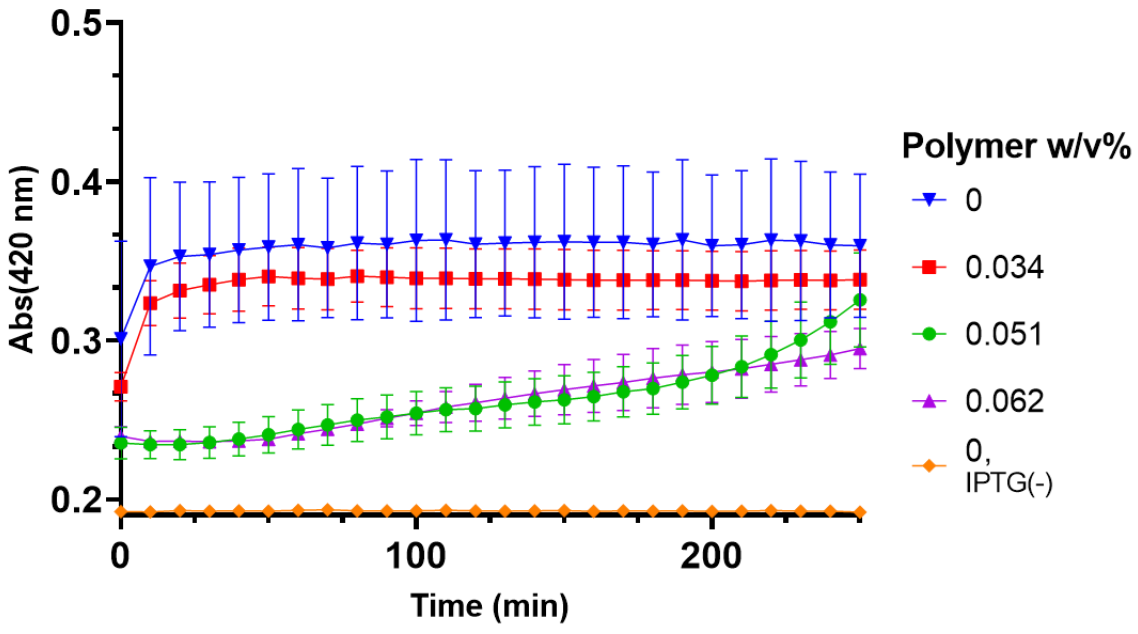

SI Figure 7. Absorbance of ABTS radical cations by Mb-harbouring bacteria, showing the slowing effect of the membrane for the external metabolites, and the absence of oxidation without Mb production. Data displayed as mean ±S.D., n= 3. Some error bars too small to be displayed

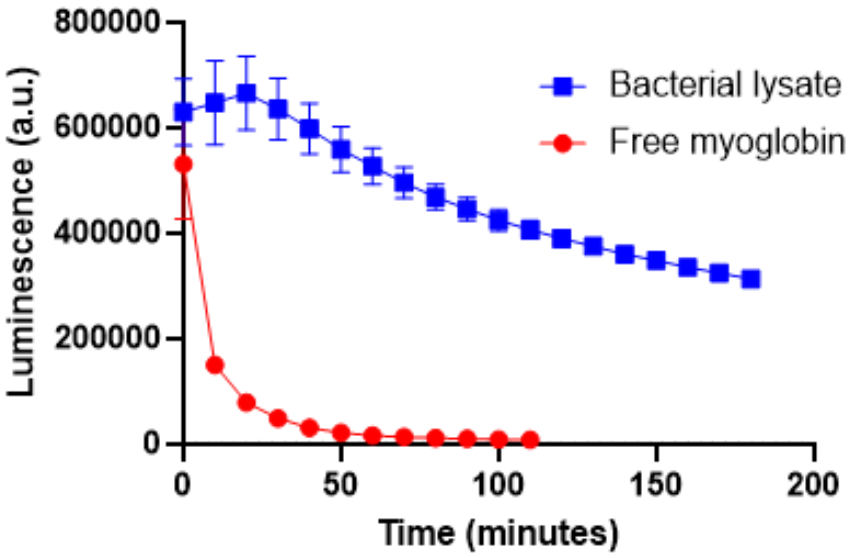

SI Figure 8. Luminescence profile derived from luminol oxidation in presence of free Mb and bacterial lysate after Mb expression, showing the high values quickly reached in the mixture and the decay coming from the peroxidation of the product, which does not happen when the diffusion is slower and controlled. Data displayed as mean ±S.D., n= 3. Some error bars too small to be displayed.

Whole-cell 2,4,6-trichlorochlorophenol detoxification

2,4,6-trichlorophenol (2,4,6-TCP) can be metabolized to the more electronegative product 2,6-dichloroquinone (2,6-DCQ), which can be further oxidized to its less toxic hydroxyquinone derivative (2,6-DCQOH) at high concentration of ROS (SI Figure 8a).[25] H_2O_2 was supplied to naked bacteria and E.coli@0.62% bacteria, either in one shot, or gradually via a glucose/glucose oxidase (GOX) feed. The absorbance of 2,4,6-TCP decreased quickly when the peroxide was directly supplied (SI Figure 8b), independent of the encapsulation, indicating that a high initial concentration of peroxide enhanced the activity of

Mb. The amount of the intermediate 2,6-DCQ (SI Figure 8c) was not affected by either encapsulation or H_2O_2 source, suggesting that its production was independent of these two factors. Interestingly, the highest production of 2,6-DCQOH was detected when GOX provided the peroxide to E.coli@0.62%, and the second highest for GOX+naked bacteria (SI Figure 8d). From this result, we can infer that the rapid addition of H_2O_2 enhances the removal of 2,4,6-TCP, compared to the use of GOX. However, the resulting 2,6-DCQ is not oxidized further, as even the PL121 membrane fails to counter the combined toxicity of the model pollutants and the peroxide. Instead, with a GOX-Mb cascade, 2,6-DCQ is transformed more easily in the less toxic 2,6-DCQOH, with E.coli@0.62% showing the highest transformation of all. The growth of bacteria, i.e. their survival, was correlated with the production of 2,6-DCQOH (SI Figure 8e). From the perspective of the membrane, it did not improve the outright removal of 2,4,6-TCP, but it acted as a barrier, allowing a slow and constant flow of both H_2O_2 and chlorophenols which, in conjunction with GOX, made the encapsulated bacteria capable of detoxifying 2,4,6-TCP until the end of the cascade, and the bacteria more able to increase their biomass.

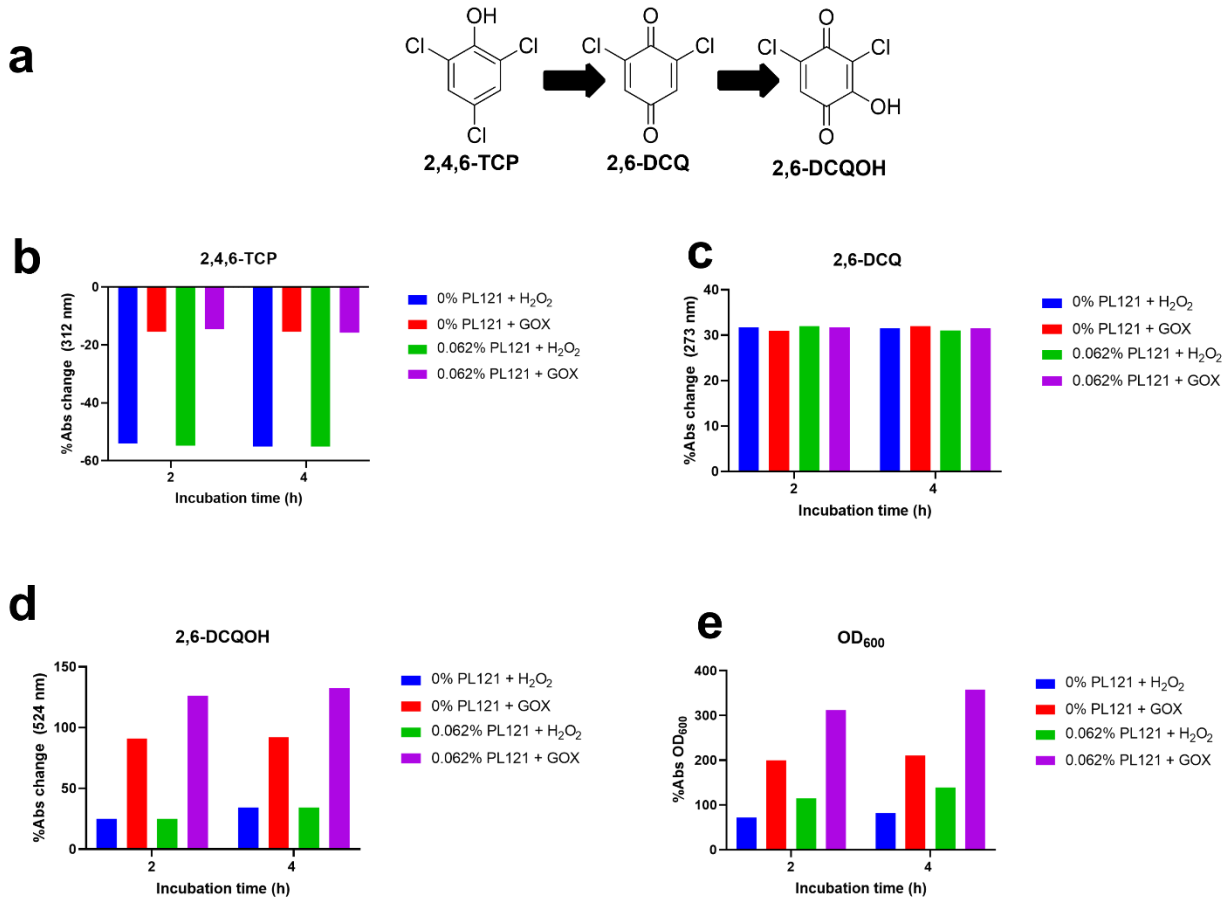

SI Figure 9 a) Reaction scheme of the reaction leading from the very toxic 2,4,6-TCP to the less harmful 2,6-DCQOH b) % variation of the absorbance typical for 2,4,6-TCP over time. c) % variation of the absorbance typical for 2,6-DCQ over time. d) % variation of the absorbance typical for 2,6-DCQOH over time. e) % variation of the OD_{600}, showing how the slower production and diffusion of hydrogen peroxide favors the production of 2,6-DCQOH and bacterial proliferation alike.

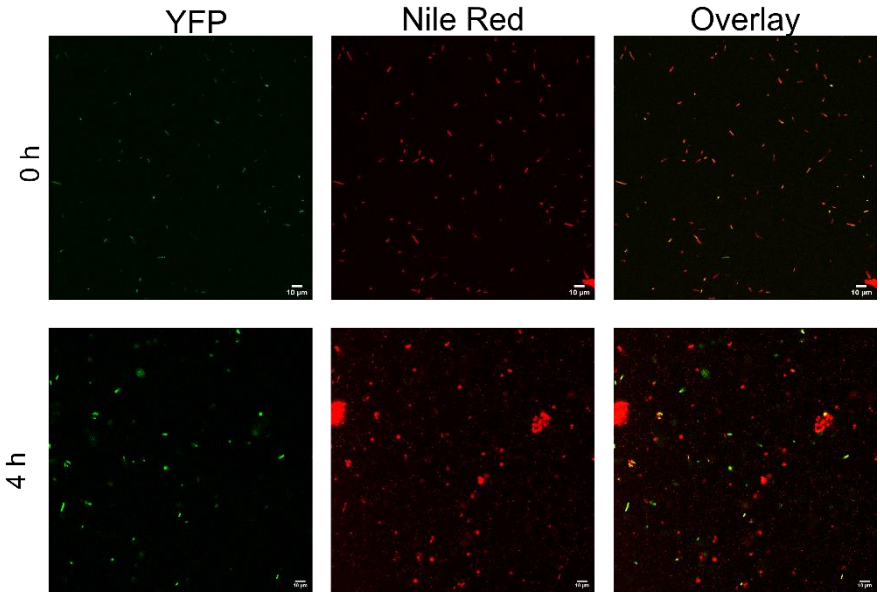

SI Figure 10. CLSM micrographs of YFP bacteria, with the lipid stain Nile Red, highlighting both fluorescent and non-fluorescent bacteria, showing the appearance of cell debris (and a higher frequency of fluorescent bacteria) after incubation with lysozyme for 4 h.

[1] K. J. D. Lee, S. E. Marcus, J. P. Knox, *Molecular Plant* **2011**, *4*, 212-219.

[2] a) V. Krzyzanek, N. Sporenberg, U. Keller, J. Guddorf, R. Reichelt, M. Schönhoff, *Soft Matter* **2011**, *7*, 7034-7041; b) J. Gaitzsch, X. Huang, B. Voit, *Chemical Reviews* **2016**, *116*, 1053-1093; c) M. V. Zyuzin, A. S. Timin, G. B. Sukhorukov, *Langmuir* **2019**, *35*, 4747-4762; d) C. B. Giuliano, N. Cvjetan, J. Ayache, P. Walde, *ChemSystemsChem* **2021**, *3*, e2000049; e) M. G. Gouveia, J. P. Wesseler, J. Ramaekers, C. Weder, P. B. V. Scholten, N. Bruns, *Chem. Soc. Rev.* **2022**.

[3] a) H. G. Sundararaghavan, J. A. Burdick, in *Comprehensive Biomaterials* (Ed.: P. Ducheyne), Elsevier, Oxford, **2011**, pp. 115-130; b) A. Rodrigo-Navarro, S. Sankaran, M. J. Dalby, A. del Campo, M. Salmeron-Sanchez, *Nature Reviews Materials* **2021**, *6*, 1175-1190.
[4] H. Lee, N. Kim, H. B. Rheem, B. J. Kim, J. H. Park, I. S. Choi, **2021**, *10*, 2100347.
[5] J. J. Huang, in *Retinal Pharmacotherapy* (Eds.: Q. D. Nguyen, E. B. Rodrigues, M. E. Farah, W. F. Mieler), W.B. Saunders, Edinburgh, **2010**, pp. 81-85.
[6] a) J. Lu, W. Peng, Y. Lv, Y. Jiang, B. Xu, W. Zhang, J. Zhou, W. Dong, F. Xin, M. Jiang, *Industrial & Engineering Chemistry Research* **2020**, *59*, 17026-17034; b) I. Moya-Ramírez, P. Kotidis, M. Marbiah, J. Kim, C. Kontoravdi, K. Polizzi, *ACS Synthetic Biology* **2022**, *11*, 1303-1312.
[7] a) T. G. Johnston, S.-F. Yuan, J. M. Wagner, X. Yi, A. Saha, P. Smith, A. Nelson, H. S. Alper, *Nature Communications* **2020**, *11*, 563; b) H. Priks, T. Butelmann, A. Illarionov, T. G. Johnston, C. Fellin, T. Tamm, A. Nelson, R. Kumar, P.-J. Lahtvee, *ACS Applied Bio Materials* **2020**, *3*, 4273-4281.
[8] S. D. Ling, Y. Geng, A. Chen, Y. Du, J. Xu, *Biomicrofluidics* **2020**, *14*, 061508.
[9] F. Shao, L. Yu, Y. Zhang, C. An, H. Zhang, Y. Zhang, Y. Xiong, H. Wang, **2020**, *8*.
[10] D. Vona, S. R. Cicco, R. Ragni, C. Vicente-Garcia, G. Leone, M. M. Giangregorio, F. Palumbo, E. Altamura, G. M. Farinola, *Photochemical & Photobiological Sciences* **2022**.
[11] a) S. S. Balkundi, N. G. Veerabadran, D. M. Eby, G. R. Johnson, Y. M. Lvov, *Langmuir* **2009**, *25*, 14011-14016; b) Y. J. Eun, A. S. Utada, M. F. Copeland, S. Takeuchi, D. B. Weibel, *ACS chemical biology* **2011**, *6*, 260-266; c) R.-B. Song, Y. Wu, Z.-Q. Lin, J. Xie, C. H. Tan, J. S. C. Loo, B. Cao, J.-R. Zhang, J.-J. Zhu, Q. Zhang, *Angewandte Chemie International Edition* **2017**, *56*, 10516-10520; d) T. Harimoto, J. Hahn, Y.-Y. Chen, J. Im, J. Zhang, N. Hou, F. Li, C. Coker, K. Gray, N. Harr, S. Chowdhury, K. Pu, C. Nimura, N. Arpaia, K. W. Leong, T. Danino, *Nature Biotechnology* **2022**; e) S. Peil, S. J. Beckers, J. Fischer, F. R. Wurm, *Materials Today Bio* **2020**, *7*, 100061; f) J. Pan, G. Gong, Q. Wang, J. Shang, Y. He, C. Catania, D. Birnbaum, Y. Li, Z. Jia, Y. Zhang, N. S. Joshi, J. Guo, *Nature Communications* **2022**, *13*, 2117.
[12] a) L. Wang, Y. Li, X.-Y. Yang, B.-B. Zhang, N. Ninane, H. J. Busscher, Z.-Y. Hu, C. Delneuville, N. Jiang, H. Xie, G. Van Tendeloo, T. Hasan, B.-L. Su, *National Science Review* **2021**, *8*, nwaa097; b) H. Lee, J. Park, N. Kim, W. Youn, G. Yun, S. Y. Han, D. T. Nguyen, I. S. Choi, **2022**, *34*, 2201247.
[13] J. Li, C. Zheng, B. Liu, T. Chou, Y. Kim, S. Qiu, J. Li, W. Yan, J. Fu, *Nanotechnology* **2018**, *29*, 365705.
[14] Z. Cao, S. Cheng, X. Wang, Y. Pang, J. Liu, *Nature Communications* **2019**, *10*, 3452.
[15] A. M. Bodratti, P. Alexandridis, *Expert Opinion on Drug Delivery* **2018**, *15*, 1085-1104.
[16] T. Foster, K. D. Dorfman, H. T. Davis, *Langmuir* **2010**, *26*, 9666-9672.
[17] M. Houbrechts, L. Caire da Silva, A. Ethirajan, K. Landfester, *Soft Matter* **2021**, *17*, 4942-4948.
[18] R. Luo, K. Göpfrich, I. Platzman, J. P. Spatz, *Advanced Functional Materials* **2020**, *30*, 2003480.
[19] A. Belluati, V. Mikhalevich, S. Yorulmaz Avsar, D. Daubian, I. Craciun, M. Chami, W. P. Meier, C. G. Palivan, *Biomacromolecules* **2020**, *21*, 701-715.
[20] D. F. do Nascimento, L. R. Arriaga, M. Eggersdorfer, R. Ziblat, M. d. F. V. Marques, F. Reynaud, S. A. Koehler, D. A. Weitz, *Langmuir* **2016**, *32*, 5350-5355.
[21] F. Itel, M. Chami, A. Najer, S. Lörcher, D. Wu, I. A. Dinu, W. Meier, *Macromolecules* **2014**, *47*, 7588-7596.
[22] S. Bhusari, S. Sankaran, A. del Campo, *Advanced Science* **2022**, *9*, 2106026.
[23] P. Alexandridis, T. Nivaggioli, T. A. Hatton, *Langmuir* **1995**, *11*, 1468-1476.
[24] Z. Song, L. Wang, S. Hou, *Analytical and bioanalytical chemistry* **2004**, *378*, 529-535.
[25] a) Z. Pan, Z. Du, J. Jia, A. Lin, Y. Wang, W. Song, S. Sun, H. Wang, R. Jia, L. Hou, *Chemosphere* **2022**, *296*, 134014; b) S. Franzen, K. Sasan, B. E. Sturgeon, B. J. Lyon, B. J. Battenburg, H. Gracz, R. Dumariah, R. Ghiladi, *The Journal of Physical Chemistry B* **2012**, *116*, 1666-1676.

[26] K. A. Davis, P.-J. Wu, C. F. Cahall, C. Li, A. Gottipati, B. J. Berron, *Journal of Biological Engineering* **2019**, *13*, 5.
[27] a) V. Maffeis, A. Belluati, I. Craciun, D. Wu, S. Novak, C.-A. Schoenenberger, C. G. Palivan, *Chemical Science* **2021**, *12*, 12274-12285; b) A. Belluati, I. Craciun, C. G. Palivan, *ACS Nano* **2020**, *14*, 12101-12112; c) A. Belluati, I. Craciun, J. Liu, C. G. Palivan, *Biomacromolecules* **2018**, *19*, 4023-4033.
[28] a) M. Raha, I. Kawagishi, V. Müller, M. Kihara, R. M. Macnab, *Journal of bacteriology* **1992**, *174*, 6644-6652; b) J. K. Roy, A. Borah, C. L. Mahanta, A. K. Mukherjee, *Journal of Molecular Catalysis B: Enzymatic* **2013**, *97*, 118-129.
[29] a) R. J. Atterbury, J. Tyson, **2021**, *167*; b) C. J. Harding, S. G. Huwiler, H. Somers, C. Lambert, L. J. Ray, R. Till, G. Taylor, P. J. Moynihan, R. E. Sockett, A. L. Lovering, *Nature Communications* **2020**, *11*, 4817.
[30] N. Bruns, K. Pustelny, L. M. Bergeron, T. A. Whitehead, D. S. Clark, **2009**, *48*, 5666-5669.
[31] S. C. Gill, P. H. von Hippel, *Analytical Biochemistry* **1989**, *182*, 319-326.